Caving 2022 - Y Potvin (ed.)

doi:10.36487/ACG_repo/2205_71

Development of rock mass strength block models at Cadia East mine

ME Pierce *Pierce Engineering, USA*

P Stonestreet *Newcrest Mining Limited, Australia*

C Orrego *Newcrest Mining Limited, Australia*

D Tennant *Newcrest Mining Limited, Australia*

TV Garza-Cruz *Itasca Consulting Group, Inc., USA*

J Furtney *Itasca Consulting Group, Inc., USA*

C Thielsen *Itasca Consulting Group, Inc., USA*

Abstract

Block models of rock mass strength have been developed at Cadia East mine to support forecasting of excavation performance. This paper describes four key aspects of the workflow that have enabled forecasting of rock mass strength throughout the entire orebody: 1) high density measurements of the spatial variability in intact and defected rock strength, derived from systematic point load testing of core from select boreholes; 2) continuous estimates of core-scale rock strength along all boreholes (including those with no or low density testing), enabled by application of machine learning to all available geological and geotechnical data, 3) estimation of tunnel-scale rock mass strength from the local statistical distribution of core-scale strengths, enabled by synthetic rock mass (SRM) testing, and 4) development of an integrated litho-structural model and the implementation of a structural trend to estimate block variables.

Keywords: *cave mining, systematic point load testing, machine learning, synthetic rock mass, rock mass strength, block modelling*

1 Introduction

Understanding the spatial variation in rock mass strength is critical to many aspects of geotechnical mine design, including excavation and ground support design. This is particularly relevant in the hydrothermally altered rocks at Cadia East mine, a panel caving operation located near Orange, New South Wales, Australia. As with other alkalic and calc-alkalic porphyry deposits, the rock at Cadia East exhibits significant spatial variability in the style of alteration (i.e. nature of mineralogical replacements), intensity of alteration (amount of replacement), vein mineralogy, and vein strength (Fox 2012). At least six different vein families are present, the most dominant of which is a sheeted vein set comprised of quartz-calcite-sulfide veins associated with mineralisation. Other widespread vein sets are composed of quartz-magnetite and calcite-hematite-laumontite, while epidote-calcite-prehnite veins can be found in the inner and outer propylitic alteration zones and calcite-illite-pyrite veins can be found in close proximity to pyrite faults. As with other deep deposits of this sort, structure is dominated by these vein sets, with only sparse open jointing.

The alteration and veining result in a rock strength that exhibits significant variability, over scales ranging from the centimetre to deposit scale and makes it difficult to apply traditional domaining techniques employing lithology in combination with alteration assemblage. In most cases, the intra-domain strength heterogeneity resulting from this approach is much larger than inter-domain heterogeneity. This is a hindrance to reliable forecasting of tunnel and pillar performance (and often cave-scale performance) and has motivated a move towards the production of geostatistical block models of intact strength and fracture

intensity to define rock mass strength heterogeneity. These rely on testing and mapping techniques that provide more systematic and widespread data such as point load testing (PLT), borehole imaging, photogrammetry, and hyperspectral scanning. Discrete fracture network (DFN) related workflows are also central to the production of block models of fracture intensity (e.g. Rogers et al. 2014).

One also requires an appropriate means to convert estimates of intact strength and fracture intensity into estimates of rock mass strength for use in numerical models and other geomechanical mine design tools. synthetic rock mass (SRM) testing offers the means to bridge this gap and enable the conversion of joint intensity and intact strength block models into block models of rock mass strength and fragmentation potential (e.g. see Pierce et al. 2007; Garza-Cruz & Pierce 2014). This paper documents the construction of intact strength block models for Cadia East based on the results of systematic point load testing and application of a machine learning (ML) model to make predictions of intact strength along logged core that was not tested (Thielsen et al. 2022). This is followed by a description of how SRM testing was used to link rock mass strength to the statistical descriptors of intact strength captured within the block modelling process, enabling conversion of the intact strength block model to a rock mass strength block model.

2 Rock strength testing, estimation and statistical analysis

The intact and defected rock strength at Cadia East was measured directly via systematic point load testing and also was estimated in untested sections of core through the use of ML enabled strength classification. With this approach, it was possible to greatly expand the volume of strength data for use in block modelling of intact strength. This section reviews the testing and estimation techniques and the resulting statistical distributions of intact and vein strength used for input to SRM testing.

2.1 Systematic point load testing

Systematic point load testing was used as a means to quantify the variability in both intact and structural tensile strength at Cadia East over the largest possible volume with a minimum of bias. It involves performing point load tests at strict 1–2 m intervals along core from multiple boreholes and taking care to recognise both structure (which requires careful alignment of the test platens) and core disturbance at the testing locations. A disturbed condition indicates that it is not possible to obtain a sample containing the test location mark that is also of valid dimension and character. This can be due to the presence of single or multiple existing open fracture(s) through intact rock or structure that are not the result of a purposefully induced break (e.g. at the end of a core run or to fit the core into the box). Test locations designated as disturbed are considered as an indicator of low point load index. The procedures, first applied to the study of rock strength variability at Niobec Mine in November of 2012 (Pierce 2014; Garza-Cruz & Pierce 2016) have since been applied to a number of orebodies, including Cadia East, Red Chris, Ghaghoo, Renard, Henderson, Eleonore, and Westwood (Bouzeran et al. 2019). See Appendix for more detail on the procedure and data types collected.

2.1.1 Failure type analysis

Systematic point load testing was carried out on 19 holes at Cadia East at a strict spacing of either 1 or 2 m, resulting in approximately 8,757 test locations. The core was marked as disturbed at 23% of the test locations, resulting in the recording of 2,060 point load indices with a value equal to zero (Figure 1). Diametral tests were conducted at the remaining locations, of which 17% (1,450 tests) were deemed invalid. Of the 5,247 valid diametral tests, break type was roughly equally divided amongst intact rock (single or multiple fractures), structure (single vein or microdefect) and combined (intact and structure). Whisker plots of point load index by break type show a wide range in strengths for both intact and structural breaks, with a coefficient of variance close to unity and structural breaks exhibiting a mean strength approximately half that of the intact breaks (Figure 2). The intact breaks also exhibit a more symmetric distribution than the structural breaks, which are skewed toward zero.

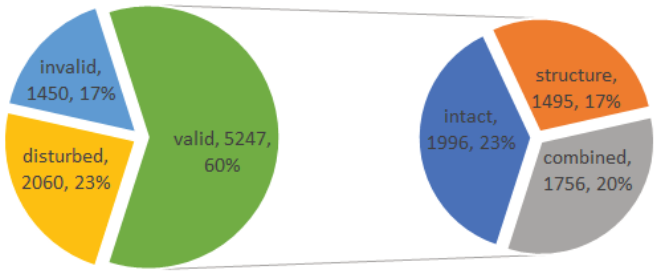

Figure 1 Breakdown of systematic point load test outcomes (left) and break types (right) from Cadia East

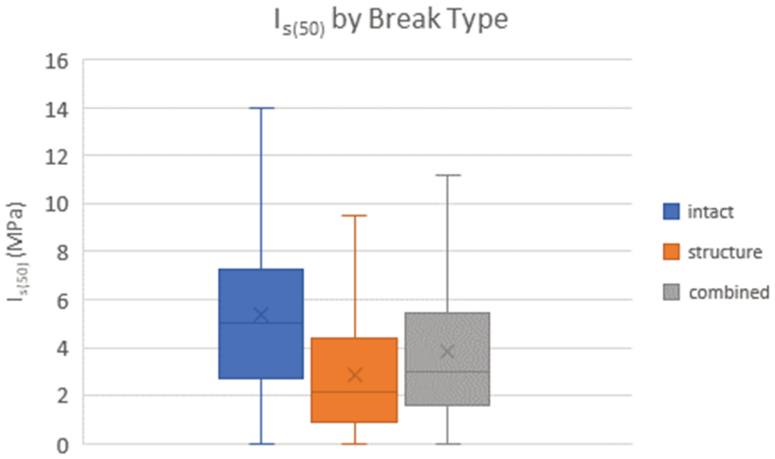

Figure 2 Whisker plot of point load indices by failure type from systematic point load testing at Cadia East

2.1.2 Downhole trends

In order to illustrate the variability in intact strength revealed by the point load testing, downhole moving averages of more than 10 non-zero point load indices were converted to UCS estimates using the typical range suggested by the International Society for Rock Mechanics (ISRM 1989) (i.e. UCS = 20 - 25 × Is50). An example borehole from Cadia East is shown in Figure 3. It reveals a strong spatial variability in UCS over multiple length scales that includes the impact of all structures and defects encountered during testing.

Variogram analysis of the point load data reveals a very strong nugget effect on the order of 60%. While some of this near-field variability in tensile strength could be attributed to the nature of the point load test method and associated sampling error, examination of core before, during, and after testing and the nature of the failures suggests that it can mostly be attributed to the natural variability induced by the presence of veins, defects, open fractures, and alteration. Two larger scales of strength variability on the order of 25 and 130 m are also revealed by the variogram analysis.

Correlations between point load index and all available logged quantities, including lithology and alteration facies, were generally very weak. When ML tools (random forest classification) were applied to the problem, a complex interplay of several key geotechnical, structural, and mineralogical factors were revealed (Thielsen et al. 2022), along with the importance of considering additional engineered features such as alteration strength index (Wyering et al. 2015).

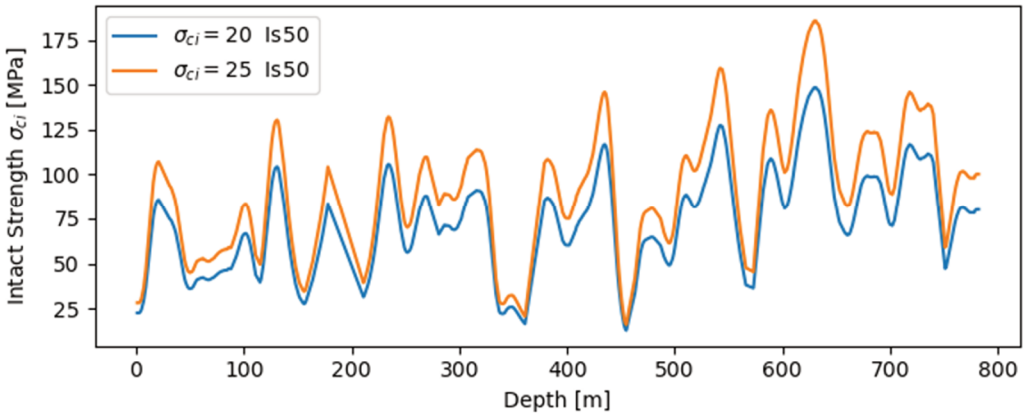

Figure 3 Example of downhole variability in UCS estimated from a rolling average of systematic point load indices from systematic testing at Cadia East

2.2 Intact strength estimation via ML

The systematic PLT data collection at Cadia East covered only 1.3% of the 590 km of holes logged at Cadia East and so ML was used to train models using the PLT data that was already collected and make predictions of intact and defected rock strength for the remaining logged core that was not tested. As described by (Thielsen et al. 2022), a procedure was first developed to homogenise the available geotechnical and geological logging data, infill missing values, and encode raw data into engineered features for use in a ML model. A random forest classifier was then trained from the collected PLT data and logging data, and applied to estimate point load index (Is50) from core logging data where point load tests were not performed. The random forest model predicts the rolling average of actual Is50 values from systematic testing within 1 MPa 48% of the time. The model also gives insights into which core logging quantities have the strongest controls on rock strength and provides the basis for developing more detailed geospatial models of intact and defected rock strength.

2.3 Statistical analysis of strength data

The Weibull distribution is used to describe the distribution of point load index due to its versatility and flexibility. The probability density function (PDF) and cumulative density functions (CDF) are defined as follows:

$$\text{PDF: } F(x) = (\beta/(\eta^{\beta}))\,(x^{(\beta-1)})\,(\exp[-((x/\eta)^{\beta})]) \quad (1)$$

$$\text{CDF: } F(x) = 1-\exp(-((x/\eta)^{\beta})) \quad (2)$$

where β is the shape parameter, also known as the Weibull slope, and η is the scale parameter. The scale parameter corresponds to the 63.2 percentile of the data, while the shape parameter describes the shape of the distribution. A low shape parameter corresponds to a distribution that is skewed towards the left while a high scale parameter results in a more symmetric distribution, similar to a normal distribution. More specifically, a Weibull shape parameter of 1.0 represents an exponential distribution, a shape parameter of 2.0 is a Raleigh distribution and a Weibull shape parameter of about 3.0 or above represents an approximately normal distribution.

Weibull fits to the non-zero measured and ML-estimated point load indices were made over moving 30, 60 and 90 m windows down each borehole. When the scale and shape parameters are plotted downhole, a strong heterogeneity in intact strength is revealed, with the scale parameter (63rd percentile) varying from ≈1–7 MPa over a distance of less than 90 m (Figure 4a). A plot of the percentage of zero strength indices reveals a similarly high heterogeneity in the degree of fracturing, varying from 10-60% over similar distances (Figure 4b). Smaller scales of observation exhibit more variability, as would be expected. Table 1 summarises the quartiles associated with 30-m window fits at Cadia East.

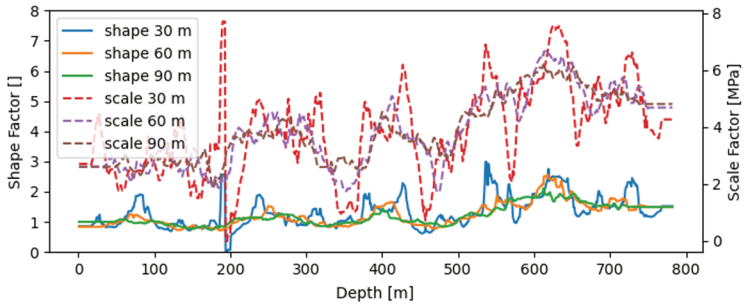

(a)

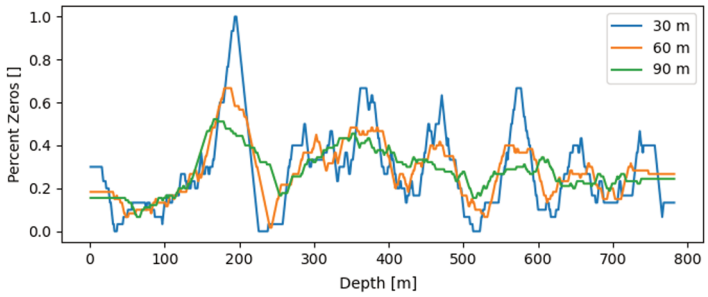

(b)

Figure 4 **Example of downhole trends in (a) Weibull parameters (scale and shape parameters) at Cadia East from fitting of point load indices over various window sizes and (b) corresponding percentage of zero strength measures**

Table 1 **Lower, middle, and upper quartile Weibull parameters fitted to a 30 m window of Cadia East PLT data**

	25th percentile	50th percentile	75th percentile
Is50 scale parameter, intact breaks (MPa)	4.14	5.47	6.61
Is50 shape parameter, intact breaks (MPa)	1.64	2.21	3.11
Is50 scale parameter, structural breaks (MPa)	1.92	2.85	3.85
Is50 shape parameter, structural breaks (MPa)	1.04	1.41	2.02
% structural breaks	29%	42%	57%
% pre-existing breaks	17%	27%	37%
Is50 scale parameter, intact breaks (MPa)	4.14	5.47	6.61

3 Rock mass strength estimation

It is often feasible to use the Hoek–Brown-GSI (HB-GSI) approach for the estimation of strength in intensely jointed rock (Hoek & Brown 2019), since this approach assumes that the rock blocks themselves do not fracture and the rock mass has low to no tensile strength. At low to moderate levels of joint intensity, however, only a portion of the in situ rock volume is comprised of joint-bounded blocks and joint slip must be accompanied by the development of new fractures in order for the rock mass to yield and disintegrate. Where joints are absent or widely spaced relative to the scale of the excavation, as is the case for Cadia East rock mass at the tunnel scale, rock masses fail via stress fracturing alone in a brittle manner and the

Hoek–Brown approach is no longer valid. SRM testing was selected as the means to characterise strength under these conditions as it can simulate both joint slip and new fracture growth (including spalling). Emergent behaviour is dependent on the scale of the sample, the specific patterns, properties, and continuity of embedded persistent structure, and the distribution of intact strength as controlled by more impersistent veining and alteration.

3.1 Synthetic rock mass testing

While the term SRM was originally defined by Pierce et al. (2007) as referring to three-dimensional DEM-based models of rock with embedded DFNs, the term is now applied to a much wider range of both 2D and 3D numerical approaches, suggestive of any model (continuum to hybrid to DEM) that attempts to represent intact rock or jointed rock masses in a more realistic way through the inclusion of flaws at any scale (e.g. grain boundaries, clasts, veins). SRM samples were developed for Cadia East rock mass using the 3DEC-based bonded block modelling (BBM) approach of Garza-Cruz & Pierce (2014), where the veined intact rock matrix is represented by tetrahedral-shaped elastic blocks and a high variance in contact strength informed by point load testing. The Cadia East samples were 9 m in diameter by 18 m high and comprised of deformable tetrahedral blocks with a 0.5 m edge length. They were numerically tested under uniaxial conditions as well as in direct tension to obtain the emergent large-scale uniaxial compressive strength and emergent tensile strength. The strengths emerging from these tests are considered representative of the rock mass at the tunnel to crusher chamber scale due to the scale of the samples tested (9 m diameter) and the fact that more persistent features (veins, joints, faults) impacting the rock mass at larger scales are excluded.

3.1.1 Input properties

Point load indices are indirect measures of tensile strength and can be converted to direct tensile strengths (DTS) for use in the model by the following empirical relation (ISRM 1989):

$$DTS = Is50*1.25 \quad (3)$$

The above relation has been found to result in DTS consistent with what can be inferred from Brazilian testing (Nicksiar & Martin 2013). The cumulative direct tensile strength distributions were directly used as input to populate the BBM models. The strength of the contacts between the tetrahedral blocks forming the BBM sample were directly informed by randomly sampling such cumulative tensile strength distributions (in the prescribed proportions of intact and structure), which is used to account for strength heterogeneity. A percentage of the contacts within the model were also randomly selected and assigned zero tensile and cohesive strength to account for the proportion of the point load test locations with pre-defined breaks. Table 2 summarises the upper, middle, and lower quartile Weibull parameters of the point load indices collected from systematic testing at Cadia East that were used to define the range of these parameters within the testing program.

The cohesive to tensile strength ratios and frictional characteristics of the intact rock and veins were established based on back-analysis of 34 UCS tests on Cadia East core samples involving discrete failure, on a mixture of calcite, chalcopyrite, bornite, and molybdenite veins. This was done by analysing samples that failed entirely along a single structure (discrete failure) or along a well-defined plane (in the case of intact rock) and had the failure angle recorded. By resolving the normal and shear stress on the structure, the data could be plotted in shear-normal stress space to define cohesion and friction angles, as described by Bewick (2021). A cohesive:tensile strength ratio of 1.7 was indicated for the veins by comparison of the best fit linear shear strength envelope at normal stress < 15 MPa and the median tensile strength. The mean friction angle of the veins was 60° at low normal stress and 45° at high normal stress and so a bi-linear shear strength envelope was employed, with a transition at 15 MPa normal stress. The intact rock was found to exhibit a linear shear strength envelope with a best fit friction angle of 45° and a cohesive:tensile strength ratio of 2.5. There is likely a bias towards stronger veins and intact rock in this analysis, since weak veins and intact rock tend to break during drilling and not be present in samples selected for lab testing. As a result of this, and

the fact that no scaling of properties was carried out from lab to field scale, the friction angles obtained from this back-analysis are considered upper bound values. A lower bound case was also examined in which the friction angle of all contacts was reduced to a constant value of 30° that is typical of non-dilatant, flat rock surfaces.

A summary of input properties is provided in Table 2.

Table 2 Properties used in the bonded block models for Cadia East

	Intact contacts	Structure contacts	Zero cohesion contacts
Constitutive model	Mohr	Bi-linear Mohr	Bi-linear Mohr
Basic friction angle	30°	30°	30°
Peak friction angle 1	45°	60°	60°
Residual friction angle 1	45°	60°	60°
Peak friction angle 2	–	45°	45°
Residual friction angle 2	–	45°	45°
Normal stress crossover	–	15 MPa	15 MPa
Dilation angle 1	15°	30°	30°
Dilation angle 2	–	15°	15°
Peak tensile strength	Randomly sampled from Weibull distribution of intact break strengths	Randomly sampled from Weibull distribution of structural break strengths	0
Residual tensile strength	0	0	0
Peak cohesive strength	2.5 × tensile strength	1.73 × tensile strength	0
Residual cohesive strength	0	0	0

3.1.2 Results

The results of the Cadia East BBM testing were used to develop relations between rock mass UCS (UCS_r) and tensile strength (σ_tr) and the underlying Weibull parameters (scale parameter, η, and shape parameter, β) and percentage of zero cohesion locations, pz. Both lower and upper bound estimates (UCS_rl and UCS_ru) were generated to reflect the range in vein and intact rock friction angles examined:

$$UCS\_rl = (\eta /0.8)\cdot 2.8\cdot(1+(\ln(\max(1.5, \beta)))/3)\ (1-pz) \quad (4)$$

$$UCS\_ru = (\eta /0.8)\cdot 4.1\cdot(1+(\ln(\max(1.5, \beta)))/3)\ (-(pz^2)+0.1pz+1) \quad (5)$$

$$\sigma\_tr = (\eta /0.8)\ (-0.014\beta^2+0.16\beta)\ (1.43(\min(pz,0.7))^2 - 2.43\cdot\min(pz,0.7)+1) \quad (6)$$

Figure 5 illustrates an example of the rock mass strength estimates derived for Hole UE504 from the above equations and the 30 m rolling averages of Weibull parameters and percent zeros from point load testing shown in Figure 4. These strength estimates do not consider the weakening effect of more persistent open

joints, veins, and small-scale faults that are likely to exist at Cadia East, particularly at windows of observation larger than 30 m. They are considered most representative of the tunnel/crusher chamber scale and the choice of window size (30, 60 or 90 m) relates more to the need for averaging within a domaining exercise than to the scale of engineering interest. Future work should aim to quantify the patterns, properties, and continuity of open joints, sheeted veins, and small-scale faults likely to further lower rock mass strength at larger scales (e.g. cave scale).

Even though GSI is not considered to be applicable for much of the massive, veined rock at Cadia East, it represents a useful parameter to reproduce the estimated rock mass UCS values within numerical models that use the Hoek–Brown criterion. The Hoek and Brown criterion relates GSI and the ratio of undisturbed rock mass strength (σ_c) to intact strength (σ_{ci}) as follows:

$$\sigma_c/\sigma_{ci} = \text{sqrt}(\exp(GSI-100)/9) \quad (7)$$

Estimates of lower and upper bound 'equivalent' GSI (GSI_eql, GSI_equ) were made by substituting σ_c with lower and upper bound UCS values derived from SRM testing (UCS_rl, UCS_ru) (Equations 4 and 5). σ_{ci} values were estimated for lower bound (σ_{ci} _l) and upper bound (σ_{ci} _u) cases based on the typical range in correlation factor of 20–25 (ISRM 1989) and the downhole rolling mean of the non-zero Is50 values (Is*50) over a 30 m Hamming window:

$$\sigma_{ci}\_l = 20 \cdot Is*50 \quad (8)$$

$$\sigma_{ci}\_u = 25 \cdot Is*50 \quad (9)$$

Subbing these values into Equation 7 and solving for GSI yields the following equations for lower and upper bound equivalent GSI (GSI_eql, GSI_equ):

$$GSI\_eql = 9 \cdot \ln((UCS\_rl/(20 \cdot Is*50))^2)+100 \quad (10)$$

$$GSI\_equ = 9 \cdot \ln((UCS\_ru/(25 \cdot Is*50))^2)+100 \quad (11)$$

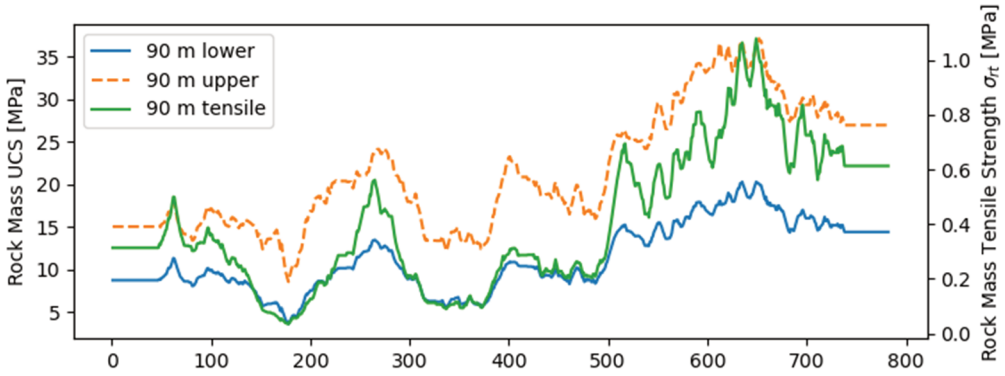

Figure 5 Example of downhole estimates of rock mass UCS and tensile strength derived from the Weibull distribution parameters and percentage zeros for Hole UE504 (Figure 4)

4 Block modelling

4.1 Database population

The drillhole database was populated with discrete values of Is50 and Is50 (non-zero) at 1 m intervals, both real and predicted. Rolling averages of the Weibull scale and shape parameters for Is50 and the percentage of zeros were also provided at each metre interval as well, for 30, 60, and 90 m moving windows. Confidence metrics were also provided for all predicted Is50 values on a scale of 0–1, with point load tested values (real) being 1 and the predicted values confidence score dependent on the completeness of the logged permutation features and their relative importance to the predictor algorithm. For block modelling, a confidence metric of 0.75 (75%) or above was selected as a conservative cut-off for data. 34% of the predicted

values achieved this confidence score, with 66% of predicted values not used for estimation. Future studies could examine the sensitivity of derived block models to this confidence cut-off.

4.2 Litho-structural model

The Cadia East litho-structural model comprises nine fault blocks and 13 recognised lithological domains. An additional geotechnical domain (calcite-laumontite fracture zones) of strongly broken ground related to post-ore genesis deformation is modelled that transcends these lithological domains. These domains formed a basis for statistical analysis of the Is50 predicted values, with average values and boundary conditions (Figure 6) resulting in 10 sub-domains being selected for the rock mass strength block model (Figure 7).

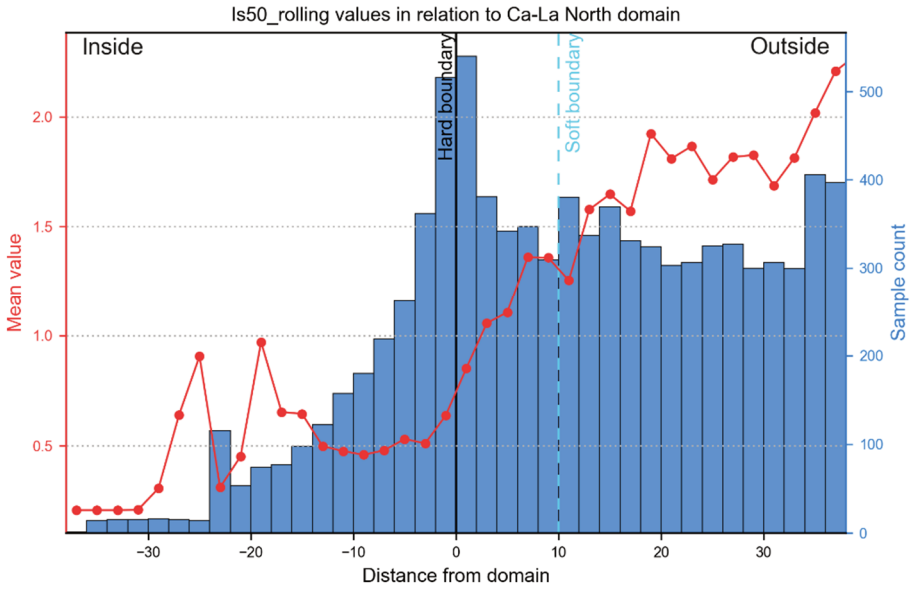

Figure 6 Plot of Is50 rolling 30 m mean values (2 m bins) inside and outside the Ca-La north subdomain, showing significantly higher Is50 values outside the subdomain with a transitional zone across the boundary. Distance from domain (x-axis) is expressed in metres

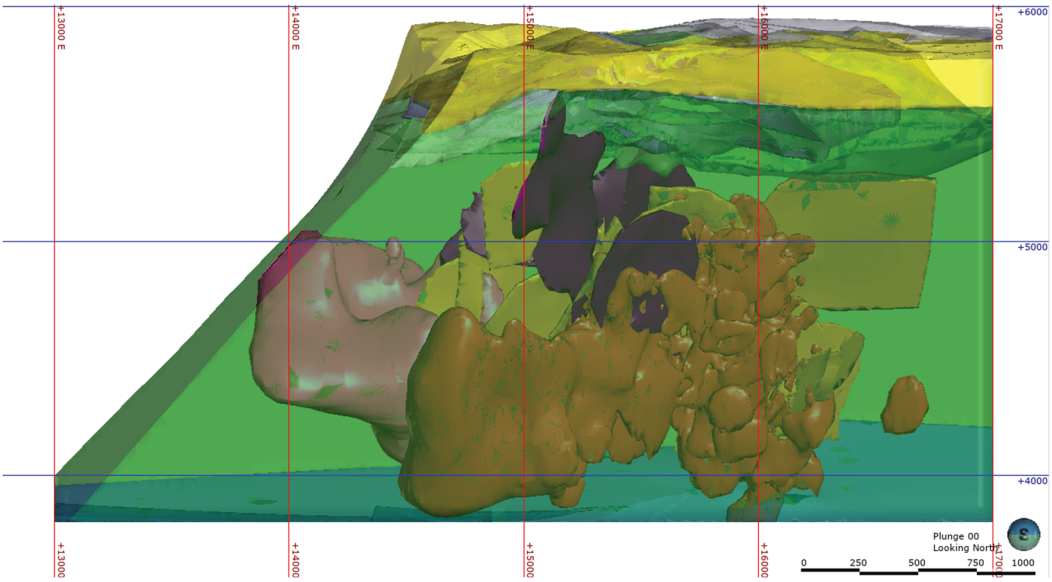

Figure 7 Long-section view of colour-coded sub-domains used for the rock mass strength model

4.3 Block modelling of point load index

4.3.1 Structural trends

The Cadia East deposit displays a strong sigmoidal-shaped trend along its length that is evident in both oriented structural (joints, faults) and mineralogical (veins) data. As four of the top five Is50 predictor features are geotechnical indicators, and three of the top 10 predictor features are mineral features, this trend was used to control the orientation of the search ellipsoid within the host volcanic units which comprise 85% of the volume of the model. Further structural trends were defined to control the orientation of the search ellipsoids in applicable sub-domains (Figure 8). Variography of each subdomain was examined to identify directions of continuity and test whether kriging was a viable method of estimation, but variography trends were only evident within the host volcanic units and agreed with the recognised structural trend.

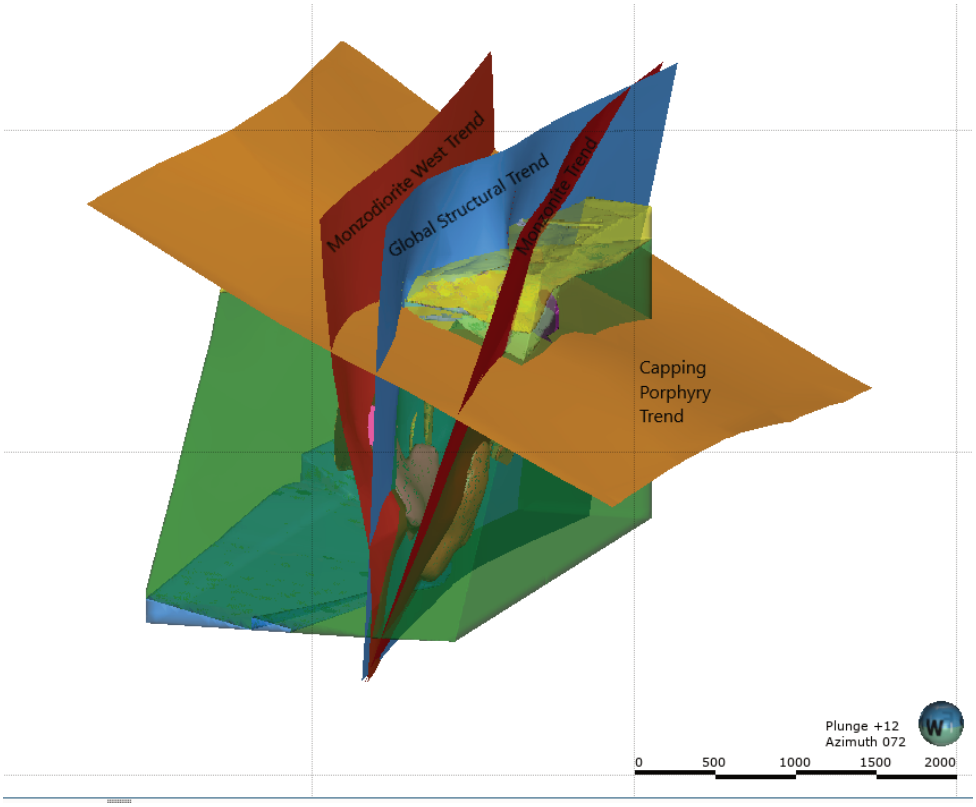

Figure 8 Structural trends used to control local variance of search ellipsoids

4.3.2 Estimation

Leapfrog Edge software was used for the estimation and block modelling process. To standardise the estimation procedure, inverse distance estimators were used across all sub-domains with the variography of the host volcanics considered when setting search ranges within that subdomain. Where applicable, the local-varying search orientation was controlled by structural trend, otherwise a static orientation was set according to the litho-structural characteristics of the subdomain. For larger domains a second search pass was performed with relaxed search inputs (longer ranges, reduction in minimum samples or drillhole limits) to populate blocks missed in the first pass. Blocks not populated by this second pass were given the mean value of the estimation parameter based on the first pass results. As data was presented as point values (downhole distance), no compositing was performed. A confidence level of 1, 2 or 3 (highest to lowest confidence) was assigned to blocks according to the average weighted distance of the block samples, with any block not populated by first or second passes automatically assigned a 3 value. Five parameters were estimated using the same search parameters specific to each subdomain (Table 3).

Table 3 Estimated and calculated parameters for the geotechnical rock mass model. All parameters estimated based on 30 m rolling window of values

Estimated parameters	Calculated parameters
Point load index, Is50	Rock mass UCS (upper and lower bound)
Non-zero point load index, Is*50	Rock mass tensile strength
Percentage of zero strength point load test locations, pz30	Equivalent GSI (upper and lower bound)
Weibull scale parameter, scale30	Intact rock strength (σ_{ci}) (upper and lower bound)
Weibull shape parameter, shape30	Confidence class

4.4 Conversion to rock mass strength block model

From the five estimated parameters in Table 3, the equations detailed in Section 3.1.2 were used to populate the block model with the calculated parameters listed in Table 3 to create the model as shown in Figure 9.

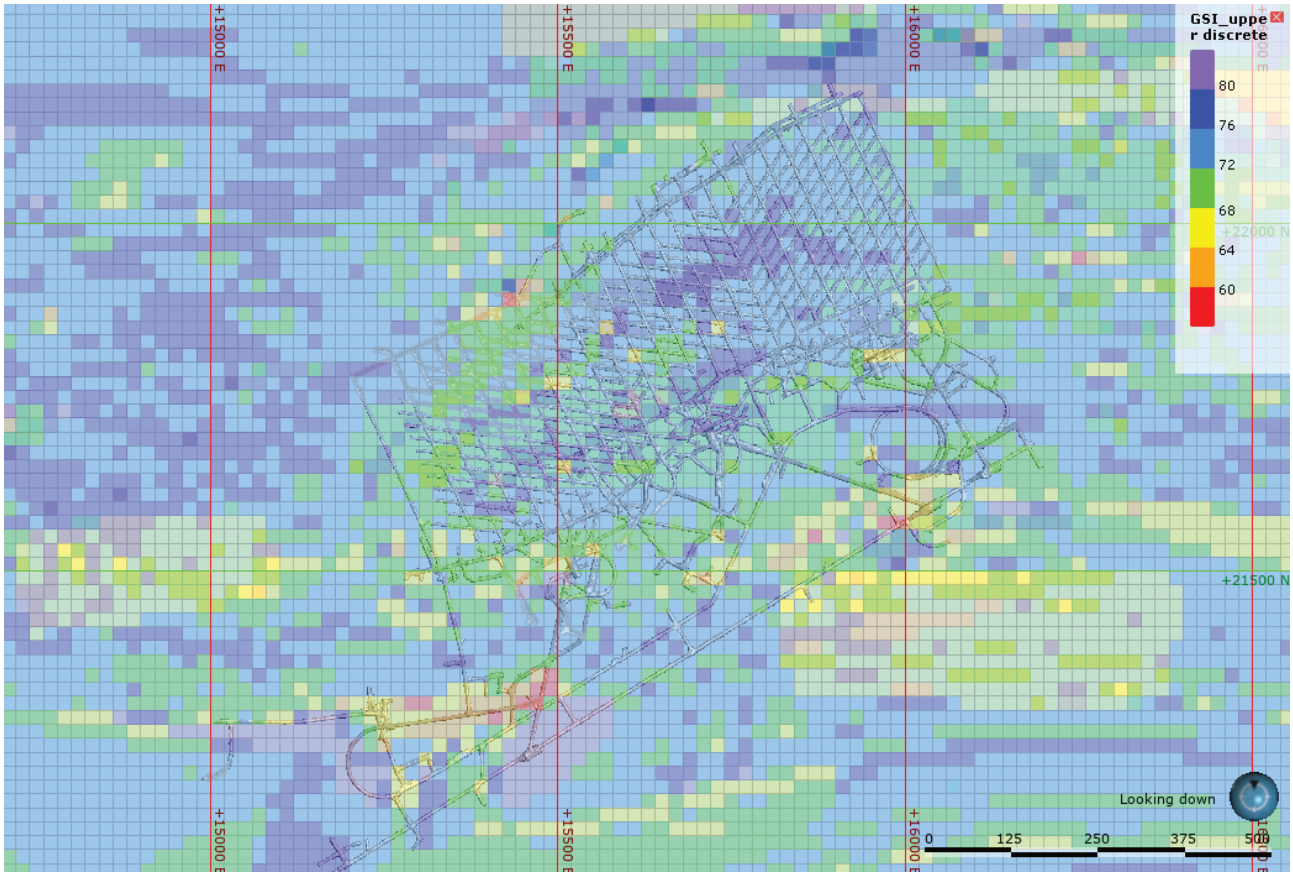

Figure 9 Horizontal slice at 4650 RL of modelled upper bound equivalent GSI values over mine development

5 Discussion

There is uncertainty associated to each step in the development of the rock mass strength block model and these should be considered when applying the rock mass strength predictions to mine design studies. For example, a certain amount of error will always be present in point load testing. This is considered acceptable in the context of a sampling program aimed at quantifying strength approximately over the widest possible area as opposed to precisely at a smaller number of discrete locations. Nevertheless, attempts should be

made in future campaigns to quantify that part of the nugget resulting from the natural geological variability within the orebody versus that which is related to sampling and testing practices (referred to as the sampling nugget effect (SNE), Dominy et al. 2001). This could be aided by the testing of reference materials with a small, known variability in strength. There is also uncertainty associated to the estimates of point load index made via application of ML at Cadia East (Thielsen et al. 2022). Sensitivity to this may be better understood by raising and lowering the cut-off value for prediction confidence (currently predictions with confidence >75% are employed in the block modelling process). Uncertainties in the SRM-derived strengths arise from how the patterns, properties and continuity of the dense vein network are represented within the models. Uncertainty in the properties has been accounted for by establishing lower and upper bound rock mass strengths from the analysis of sensitivity to vein and intact rock shear strength. Alternative models for the numerical representation of massive, veined rock could also be adopted to further explore uncertainty in this aspect.

6 Conclusion

As with other alkalic and calc-alkalic porphyry deposits, the relatively massive, veined rock at Cadia East mine exhibits significant spatial variability in the style and intensity of alteration, vein mineralogy, and vein strength. This results in a rock strength that exhibits significant variability over scales ranging from the centimetre to deposit scale, motivating the development of geostatistical block models of intact and rock mass strength. This paper demonstrated how a combination of systematic point load testing, ML, SRM testing and litho-structural modelling can be employed to generate such models for application to geomechanical mine design. The resulting models paint a more granular picture of rock mass strength than can generally be obtained from more traditional domaining approaches. This presents an opportunity to obtain more accurate forecasts of footprint stability as well as caving and fragmentation potential. Cave monitoring data can be used to test whether the spatial variability in strength estimated by the approach translates into spatial variability in undercut and extraction level performance as well as cave shape and emergent fragmentation (considering variability in other controls such as induced stress). The impacts of more widely spaced but weak and persistent sheeted veins, joints, faults, and other structures were excluded from the analysis, resulting in strength estimates most relevant to the tunnel/crusher chamber scale. This work could be extended to the cave scale by incorporating DFNs for these features into the workflow along with associated block models of their volumetric intensity.

Acknowledgement

The authors acknowledge the support of Newcrest Mining for allowing the publication of this paper and the Cadia East staff who conducted the point load testing enabling this study.

Appendix: Systematic point load testing methodology

Systematic point load testing was carried out in accordance with ISRM standards (ISRM 1989), with the exception that tests are conducted at a regular fixed spacing rather than clustered around UCS tests for the purposes of correlation. In addition, all valid tests were retained (high and low values are not discarded). Careful consideration was given to maintenance of testing points, as worn points resulted in a larger proportion of invalid tests. Testing locations were marked on the core at strict, regular intervals, using a sleeve to mark the circumference of the core. A single diametral test was conducted at each test location, with axial tests conducted periodically to check for anisotropy in the intact rock tensile strength. The spacing between point load tests was 1 m in initial holes then 2 m in later holes.

The following standard information was collected at each test site:

- Test location (distance along core).
- Test specimen description.
    - Sample type.

        - Axial or diametral.
    - Sample dimensions.
        - Diameter and length.
- Test result.
    - Peak hydraulic pressure.
    - Test validity (see ISRM 1989).

In addition, the following detailed information was gathered on core condition, test type, failure type and structure type at the test location:

- Core condition.
    - Intact: Non-defected intact rock.
    - Structure: Closed veins, foliation, bedding, microdefects.
    - Disturbed: This designates that it was not possible to obtain a sample containing the test location mark that is also of valid dimension and character. This can also be due to the presence of single or multiple existing open fracture(s) through intact rock or structure, lost core, or overly soft material at the test location. Test locations designated as disturbed were considered as an indicator of low point load index. Failure type was also noted.
- Test type.
    - Diametral: If a structure was present for a diametral test, it was aligned parallel to the testing direction so that the points lay on the structure itself. This enabled the strength of the structure to be measured. If there was no structure present, the testing direction during a diametral test was not relevant.
    - Axial.
    - None: Test not possible due to induced or disturbed core condition.
- Failure type.
    - Intact: Single fracture through intact rock only.
    - Multiple: Multiple fractures through intact rock.
    - Structure: Single fracture through structure only. The structure type (vein, foliation, bedding, microdefect) and thickness as well as the alpha angle, roughness, and mineralogy of the break surface was noted.
    - Combined: Single fracture through combination of structure and intact rock.

References

Bewick, RP 2021, 'The strength of massive to moderately jointed rock and its application to cave mining', *Rock Mechanics and Rock Engineering*, issue 8/2021, pp. 1–33.

Bouzeran, L, Pierce, M, Andrieux, P & Williams, E 2019, 'The role of rock mass heterogeneity and buckling mechanisms in excavation performance in foliated ground at Westwood Mine, Quebec', *Journal of the Southern African Institute of Mining and Metallurgy*, vol. 120, no. 1, pp. 41–48.

Dominy, SC, Johansen, GF & Annels, AE 2001, 'Bulk sampling as a tool for the grade evaluation of gold-quartz reefs', *Applied Earth Science: Transactions of the Institution of Mining & Metallurgy, Section B*, vol. 110, no. 3, pp. B176–B191.

Fox, N 2012, *Controls on Alteration and Mineralisation at the Cadia East Alkalic Porphyry Au-Cu Deposit, NSW*, doctoral dissertation, The University of Tasmania, Hobart.

Garza-Cruz, T & Pierce, M 2014, 'A 3DEC model for heavily veined massive rock masses', *Proceedings of 48th US Rock Mechanics/Geomechanics Symposium*, American Rock Mechanics Association, Alexandria.

Garza-Cruz, T & Pierce, M 2016, 'Impact of rock mass strength variability on caving', *MassMin 2016: Proceedings of the Seventh International Conference & Exhibition on Mass Mining*, Australasian Institute of Mining and Metallurgy, Melbourne.

Hoek, E & Brown, ET 2019, 'Hoek-Brown failure criterion and GSI – 2018 edition', *Journal of Rock Mechanics and Geotechnical Engineering*, vol. 11, no. 3, pp. 445–463.

ISRM 1989, *Suggested Method for Determining Point Load Strength, RTH 325-9*, ISRM, Lisbon.

Nicksiar, M & Martin, CD 2013, 'Crack initiation stress in low porosity crystalline and sedimentary rocks'. *Engineering Geology*, vol. 154, pp. 64–76.

Pierce, M, Cundall, P, Potyondy, D & Ivars, DM 2007, 'A synthetic rock mass model for jointed rock', *Proceedings of the 1st Canada-US Rock Mechanics Symposium*, American Rock Mechanics Association, Alexandria.

Pierce, M 2014, *Geomechanical Feasibility Analyses of Caving at Niobec Mine*, ICG report 13–2768–62 to Iamgold.

Rogers, S, Elmo, D, Webb, G & Catalan, A 2014, 'Volumetric fracture intensity measurement for improved rock mass characterisation and fragmentation assessment in block caving operations', *Rock Mechanics and Rock Engineering*, vol. 48, no. 2, pp. 633–649.

Thielsen, C, Furtney, J, Valencia, ME, Pierce, M, Orrego, C, Stonestreet, P & Tennant, D 2022, 'Application of machine learning to the estimation of intact rock strength from core logging data: A case study at the Newcrest Cadia East mine', *Proceedings of the 56th US Rock Mechanics/Geomechanics Symposium*, American Rock Mechanics Association, Alexandria.

Wyering, LD, Villeneuve, MC, Wallis, IC, Siratovich, PA, Kennedy, BM & Gravley, DM 2015, 'The development and application of the alteration strength index equation', *Engineering Geology*, vol. 199, pp. 48–61.